Biochimica et Biophysica Acta 1827 (2013) 769–778

Contents lists available at SciVerse ScienceDirect

Biochimica et Biophysica Acta

journal homepage: www.elsevier.com/locate/bbabio

Atomistic simulations indicate cardiolipin to have an integral role in the structure of the cytochrome bc_1 complex

Sanja Pöyry [a], Oana Cramariuc [a], Pekka A. Postila [a], Karol Kaszuba [a], Marcin Sarewicz [b], Artur Osyczka [b], Ilpo Vattulainen [a,c], Tomasz Róg [a,*]

[a] Department of Physics, Tampere University of Technology, P.O. Box 692, FI-33101 Tampere, Finland
[b] Department of Molecular Biophysics, Jagiellonian University, Kraków, Poland
[c] MEMPHYS Center for Biomembrane Physics, University of Southern Denmark, Odense, Denmark

ARTICLE INFO

Article history:
Received 17 December 2012
Received in revised form 5 March 2013
Accepted 13 March 2013
Available online 23 March 2013

Keywords:
Cardiolipin
Cytochrome bc_1
Membrane protein
Molecular dynamics simulation
Proton transfer

ABSTRACT

The reaction mechanism of the cytochrome (*cyt*) bc_1 complex relies on proton and electron transfer to/from the substrate quinone/quinol, which in turn generate a proton gradient across the mitochondrial membrane. Cardiolipin (CL) have been suggested to play an important role in *cyt* bc_1 function by both ensuring the structural integrity of the protein complex and also by taking part in the proton uptake. Yet, the atom-scale understanding of these highly charged four-tail lipids in the *cyt* bc_1 function has remained quite unclear. We consider this issue through atomistic molecular dynamics simulations that are applied to the entire *cyt* bc_1 dimer of the purple photosynthetic bacterium *Rhodobacter capsulatus* embedded in a lipid bilayer. We find CLs to spontaneously diffuse to the dimer interface to the immediate vicinity of the higher potential heme b groups of the complex's catalytic Q_i-sites. This observation is in full agreement with crystallographic studies of the complex, and supports the view that CLs are key players in the proton uptake. The simulation results also allow us to present a refined picture for the dimer arrangement in the *cyt* bc_1 complex, the novelty of our work being the description of the role of the surrounding lipid environment: in addition to the specific CL–protein interactions, we observe the protein domains on the positive side of the membrane to settle against the lipids. Altogether, the simulations discussed in this article provide novel views into the dynamics of *cyt* bc_1 with lipids, complementing previous experimental findings.

1. Introduction

The role of lipids in biological membranes and their function has earlier been undervalued, though the situation has changed quite recently [1]. Nowadays it is known that the lipids surrounding membrane proteins may have a role in proteins' stability, membrane partitioning, folding, assembly, and dynamics [2,3]. It has also been realized that lipids can modulate or even govern the function of membrane proteins [4]. For instance, there is ample evidence that generic membrane properties such as hydrophobic thickness, phase behavior, surface charge, and membrane elasticity [2,4] can influence conformations of membrane-embedded proteins. Besides these membrane-mediated interactions, individual lipids may also play a crucial role in protein function through specific binding and interaction patterns. The latter possibility is a very timely topic since recent studies by Contreras et al. have shown concretely how sphingomyelin, one of the abundant lipid types in e.g. plasma membranes, interacts specifically with certain transmembrane protein domains [5].

Further, X-ray crystallographic studies have suggested that several membrane proteins include specific phospholipid species as integral parts of their structures [6]. Some of these lipids bind to well-defined binding pockets and are a prerequisite for the structural integrity and proper function of the proteins [6]. The underlying reasons to the lipid specificity and the detailed role of the lipids in the protein function have, however, remained largely elusive. To a large extent, this is due to practical issues that limit the chances of experiments to clarify atomistic-scale phenomena associated with dynamic lipid–protein interactions.

One of the appropriate means to complement experiments is to consider complex membrane–protein systems in a purely atomistic manner through molecular dynamics (MD) simulations. This approach not only provides structural information of lipid–protein complexes but it also generates knowledge on the dynamic properties of proteins in membranes.

In this spirit, here we study the effects of lipids on the cytochrome (*cyt*) bc_1 complex (see Fig. 1) of the purple photosynthetic bacterium *Rhodobacter capsulatus* using atomistic MD simulations. The bacterial *cyt* bc_1 complex is a 6-subunit dimer, composed of *cyt b*, *cyt* c_1, and iron sulfur protein (ISP) subunits (Fig. 1A). It functions as a redox carrier in the electron transport chain, a key part of bacterial and eukaryotic energy

* Corresponding author. Tel.: +358 40 198 1010.
E-mail addresses: Ilpo.Vattulainen@tut.fi (I. Vattulainen), tomasz.rog@gmail.com (T. Róg).

0005-2728/$ – see front matter © 2013 Elsevier B.V. All rights reserved.
http://dx.doi.org/10.1016/j.bbabio.2013.03.005

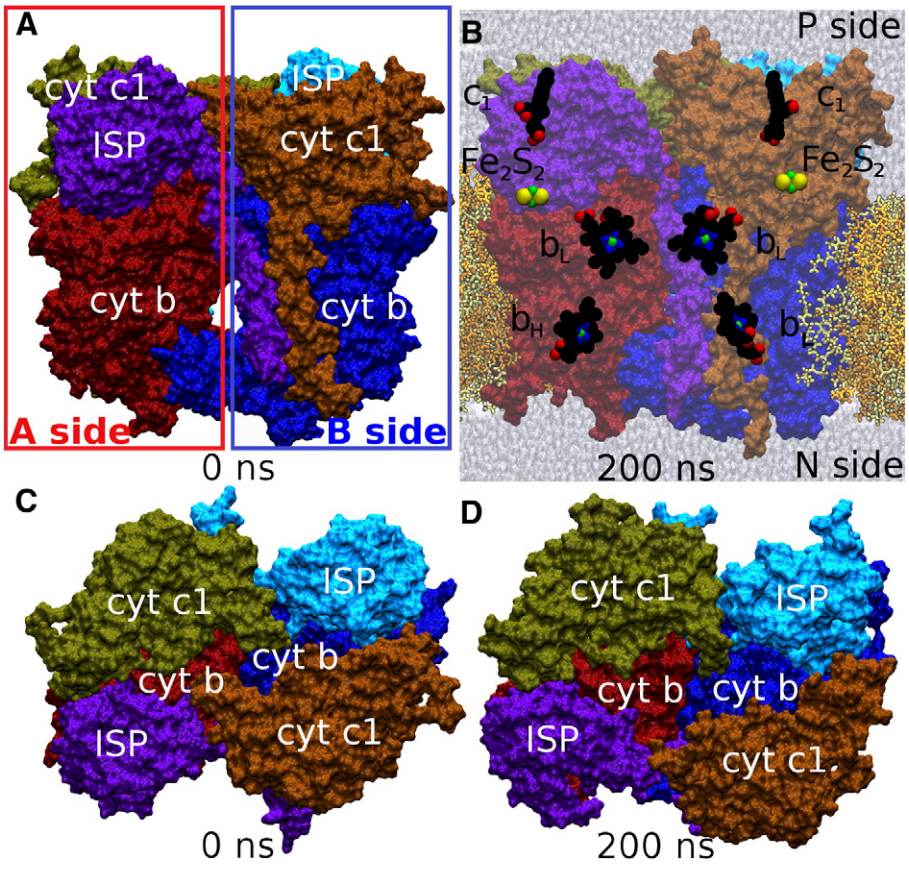

Fig. 1. The cytochrome bc_1 complex. A) The protein dimer includes cytochrome *b* (*cyt b*; red and blue), cytochrome c_1 (*cyt* c_1; yellow and orange), and iron sulfur protein (ISP; cyan and magenta) subunits shown using water-accessible surface at 0 ns. The A side of the dimer (red box) is composed of chains C (*cyt b*), D (*cyt* c_1), and R (ISP), while the B side (blue box) includes chains P (*cyt b*), Q (*cyt* c_1), and E (ISP) in the crystal structure (PDB: 1ZRT). B) The protein complex embedded in a lipid bilayer at 200 ns in the $conf_3$ simulation (Table 1) has a different conformation if compared to the state at 0 ns. The redox centers heme c_1, 2-iron 2-sulfur (Fe_2S_2) cluster, low potential heme (b_L), and high potential heme (heme b_H) are illustrated as CPK models on top of the protein. For clarity, water molecules are only shown in the background and the membrane has been clipped to reveal the protein subunits. The positive (P) side and the negative (N) sides separated by the membrane have been labeled. The Q_o site, close to the b_L heme, is located on the P side of the membrane and the Q_i-site near the heme b_H is closer to the N side of the membrane. Comparison of the top view of the complex from the P side shows that the dimer interface opens considerably between C) 0 ns and D) 200 ns. Note that most of the opening happens between the extracellular domains of *cyt* c_1 subunits.

metabolism, embedded in a cardiolipin-rich membrane (Fig. 1B). During the catalytic reaction of the *cyt* bc_1 complex (also called the Q-cycle) one quinol molecule is oxidized at the Q_o-site (that is thereby known as the oxidation site) and two electrons and protons are released. One of the electrons is delivered via the 2-iron 2-sulfur cluster (see Fig. 1B for Fe_2S_2 as part of the ISP subunit) to the heme c_1 redox center (Fig. 1B describing also part of the *cyt* c_1 subunit). Meanwhile, the other electron is routed via the low potential heme (b_L in Fig. 1B) and the high potential heme (b_H in Fig. 1B) redox centers at the Q_i-site (quinone reduction site) to reduce a non-protonated substrate quinone. Because the reaction is bifurcated, two Q-cycles are needed to produce a fully protonated substrate quinol at the Q_i-site. The proton/electron transfers to/from the substrate quinone/quinol contribute to maintaining a proton gradient across the membrane where the complex is embedded.

The presence of phospholipids has been shown to be essential for the catalytic activity and the native structure of the *cyt* bc_1 complex [7,8]. Also, the complex has been crystallized together with tightly bound cardiolipins (CLs), phosphatidylcholines (PCs), phosphatidylethanolamines (PEs), and phosphatidylinositols (PIs) [9–14]. The structural analysis of these lipid-bound complexes has been complemented by studies of lipid-dependent enzymatic activity, revealing the vital role played by the lipids [7,15,16]. Removal of the lipids has been shown to inactivate the complex, and especially CL has been found to be essential for the restoration of the enzymatic function [17,18].

With a total of four acyl chains and two negatively charged phosphate groups connected by a central glycerol group, CL has a unique double lipid structure. It is a vital component in membranes with coupled electron transport and phosphorylation, namely bacterial plasma membranes, chromatophores, chloroplasts, and mitochondria [19]. While affecting the barrier properties of the membranes, CL has also been suggested to operate at the interface between membrane proteins and their surroundings, or between the subunits of protein complexes, possibly inducing conformational changes thereby affecting their activity [20]. CL may also have a pivotal role in the higher order organization of respiratory chain's components, literally gluing the chain together [21].

Importantly, in addition to insuring the structural integrity of the *cyt* bc_1 complex, CLs have also been proposed to take part in the proton uptake at the enzyme's Q_i-site [22] and act as a proton sink [23]. More precisely, a CL molecule on the periphery of the negative (N) side of the *cyt* bc_1 complex has been proposed to function as an anionic antenna for proton uptake at the Q_i-site [22,24]. As the low potential chain (heme $b_L \rightarrow$ heme b_H) provides electrons to the substrate at the Q_i-site, the proposed picture says that the closely positioned CLs would in concert deliver protons for the non-reduced substrate forms. This theory is backed up by the facts that the acidic head groups of CL are able to carry out intramembrane proton transfer [20], and in several X-ray crystal structures of the complex (see, for example, [10,25]) CLs are positioned in the close vicinity of the Q_i-sites. Due to the difficulties in determining its charge, which depends on pH and environmental factors such as the concentration of CLs, the charge state of CL has been debated and both single and double charged cardiolipins have been proposed [23,26,27].

The objective of this work is to unravel how strongly and specifically CL interacts with *cyt* bc_1, and how these interactions are

manifested in the function of the protein complex. In this context, there are only a few computational studies that have examined the properties of CL-rich bilayers [27–30]. The present work is, to the authors' knowledge, the first simulation study focusing on CL–protein interactions. To this end, we discuss the results of four 200-ns atomistic simulations of *cyt* bc_1 in a many-component membrane comprised of CL, PC, and PE lipids.

We find lipids to play a role in a number of intriguing processes. We first find CLs to spontaneously diffuse to the protein–dimer interface to the immediate vicinity of the higher potential heme groups of the complex's catalytic (quinone reduction) Q_i-sites. This suggests that the specific CL positioning with the *cyt* bc_1 complex is highly conserved between different species. The CL positioning in the simulations close to the Q_i-sites is similar to that seen in the X-ray crystal structures of several higher level organisms such as yeast, chicken, and bovine [9–14,22,25].

The agreement of the present simulations with experiments is very promising for a number of reasons. From experimental point of view, our data provide support for the experimental approaches used to crystallize proteins of this type, since in the simulations we readily circumvent the detrimental effects caused by delipidation, crystal lattice packing, and other potential artifacts. Further, our simulation results allow us to present a refined picture for the dimer arrangement in the *cyt* bc_1 complex. The novelty of our work is the description of the role of the surrounding lipid environment: in addition to the specific CL–protein interactions, we also observe a conformational shift due to the general lipid environment, as the domains on the positive (P) side of the *cyt* bc_1 complex (see Fig. 1B) settle against the membrane. Altogether, this study represents the first atom-level perspective into the bacterial *cyt* bc_1 complex dynamics, exploring the full effect of lipids in a many-component lipid bilayer for the enzyme's structure and function.

2. Methods

2.1. System set-up

We consider four configurations ($conf_1$–$conf_4$) of the *cyt* bc_1 complex, corresponding to different states in the Q-cycle functional mechanism of the cytochrome (Table 1). Each configuration differs from the others by the redox states of the prosthetic groups and by the occupancy of the Q_o- and Q_i-sites. In the $conf_1$ simulation, the Q_o-site is not occupied by a substrate or an inhibitor (*apo*), but the Q_i-site contained semiquinol. In the $conf_2$ simulation the Q_o-site is unoccupied while antimycin, an inhibitor, is present at the Q_i-site. The $conf_3$ captures the state primed for the first turnover while $conf_4$ represents the state of the complex following immediately quinol oxidation at the Q_o-site. The details of the $conf_2$–$conf_4$ set-ups are discussed more thoroughly in our previous studies [31,32].

In each system set-up (Table 1), the *cyt* bc_1 protein dimer (PDB: 1ZRT; [33]) is embedded in a lipid bilayer, which was done using VMD [34] (Fig. 1B). All non-protein components were removed from the original PDB structure (stigmatelin) and thereby only the protein structure was used. Prior to MD simulations, the structure of the system was optimized through 500 steps of energy minimization using the conjugate gradient algorithm. In all simulation set-ups the lipid bilayer consists of three components: 102 cardiolipin (CL 18:2/18:2/18:2/18:2), 406 phosphatidylcholine (PC 18:2/18:2), and 342 phosphatidylethanolamine (PE 18:2/18:2) lipids (850 lipid molecules in total, see Fig. S1), all equilibrated in our previous studies [28,35]. This choice of lipids is particularly abundant in mitochondrial membranes [28] and is often used in experimental studies where protein complexes are reconstituted in artificial membranes. The system is fully solvated with TIP3P water molecules. For neutralizing the negative charge of the system, 246 Na^+ ions were added randomly to the water phase. The resulted systems comprise about 500,000 atoms each.

2.2. Molecular dynamics simulations

The 200 ns molecular dynamics (MD) simulations were performed with NAMD2.7 [36] using CHARMM 22 parameters for the protein with the CMAP [37] correction map for main chain dihedrals, and CHARMM 27 parameters for lipids with later modification [38]. The MD simulation set-up is described in detail in our previous work [39]. Atomic point charges for the prosthetic redox centers and ligands were fitted using the RESP methodology for both reduced and oxidized states based on extensive quantum mechanical calculations [31]. The time step was 1 fs and short-range non-bonded forces were calculated at 2 fs interval. The smooth particle mesh Ewald method was used to calculate long-range electrostatic interactions [40]. A periodic boundary box was used with dimensions of 162 Å × 142 Å × 132 Å. The protein–protein distance in the neighboring images was as a minimum two times larger than the 12 Å cut-off distance for van der Waals interactions. The target temperature was 310 K and target pressure 1 atm.

2.3. Trajectory analysis and figure preparation

The superimpositions of the protein structures were done using either VMD 1.9 or VERTAA in BODIL 0.8.1 [41]. The distance, hydrogen bonding (H-bonding), solvent accessible surface area (SASA), and electrostatic potential calculations were also performed with VMD. The distance of 3.25 Å between polar groups was used as the upper limit for H-bond formation with an angle criterion of 30°. The contacting surface area (in units of $Å^2$) between the *cyt b* and ISP subunits was assessed by performing SASA calculations. The electrostatic potential was calculated in VMD with the PMEPot plugin [42]. The figures were generated using VMD, BODIL, MOLSCRIPT 2.1.2 [43], and RASTER3D [44].

2.4. Equilibrating system configurations

As mentioned above, the starting configurations for lipid bilayers were based on our previous studies [28,35] and were thus equilibrated. When the protein was embedded to these bilayers, the lipid arrangements around the protein were therefore based on simulations of a protein-free membrane, meaning that cardiolipins and other lipids were not positioned close to the previously proposed binding sites of the protein. Important to stress is that the distance between the central binding cavity of the *cyt* bc_1 dimer (that is at the interface between the proteins, see discussion below) and the cardiolipin that was the closest

Table 1
The atomistic molecular dynamics simulation set-ups of the cytochrome bc_1 complex.

MD simulation configuration	Q_i-site inhibitor or substrate	Q_o-site substrate	Heme b_L [a]	Heme b_H [a]	Heme c_1 [a]	Fe_2S_2 cluster [a]
$conf_1$ [b]	Semiquinol	*apo*	−1 ox	−2 red	−2 red	−2 red
$conf_2$ [c]	Antimycin	*apo*	−1 ox	−1 ox	−2 red	−1 red
$conf_3$ [c]	Quinone	Quinol	−1 ox	−1 ox	−1 ox	0 ox
$conf_4$ [c]	Semiquinone	Quinone	−2 red	−1 ox	−1 ox	−1 red

[a] The formal charge of the redox centers: "red" stands for reduced, and "ox" stands for oxidized.
[b] First 100 ns of the simulation presented in Kaszuba et al. [31].
[c] Presented in Postila et al. [32].

to it was about 20–25 Å in the initial starting configuration (see Supplementary material (SM)). As the below data show, this distance decreased rapidly as the simulations were started (see Section 3.2). Further, immediately in the beginning of the simulation, the cavity at the dimer interface was filled with water molecules from the negative (N) side, but they were subsequently replaced by lipids which entered the cavity. Further discussion on equilibration is given in SM (S.1).

3. Results

3.1. Key results in a nutshell

Below we describe the results that we have found through extensive atomistic simulations. Yet, since the new knowledge we have observed is quite detailed, we consider it useful to first outline the main findings and conclusions in advance. Given this view, our four key results (in order of importance) are as follows:

1. We observed spontaneous diffusion of CL lipids to similar locations as have been earlier observed in X-ray crystallographic experiments (Fig. 2). This is a positive news for the experimental community, providing support for the protocols used in membrane protein structure determination.
2. As the role of CLs bound to the specific sites was elucidated in detail, it turned out that they were positioned very close to the active sites of the protein and indeed could participate in the proton transfer to the active sites hydrogen-bonded networks of water and lysine.
3. The space between the two protein monomers became filled up with phospholipids, thereby likely affecting the stability of the complex's structure and possibly participating in its dimer formation and quinone/quinol diffusion.
4. We also observed a conformational shift due to the general lipid environment in the *cyt* bc_1 dimer's quaternary structure, as the P side domains of the complex settled against the membrane.

We next discuss these aspects in more detail.

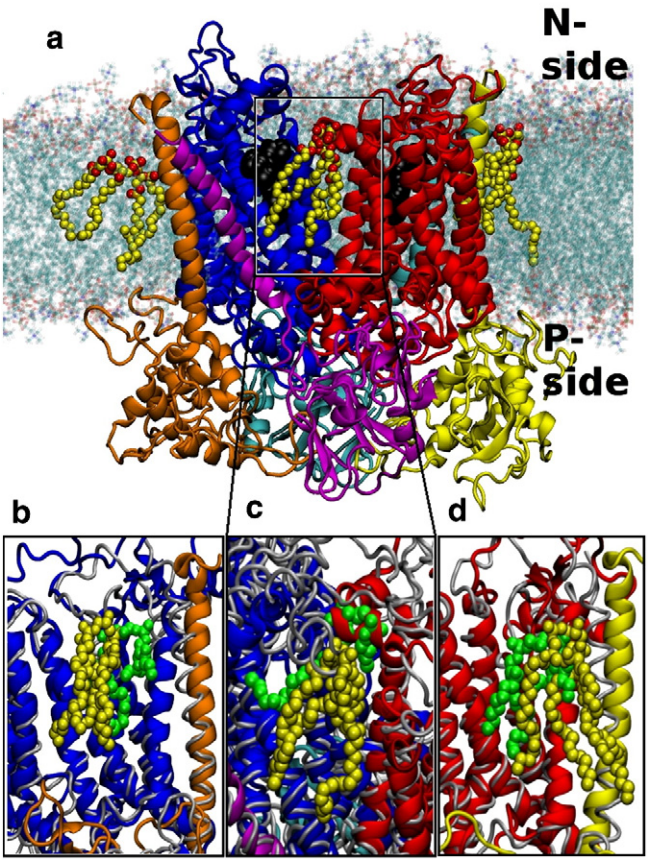

Fig. 2. Cardiolipin diffuses spontaneously to similar binding sites as observed in X-ray crystal structures. a) An example of the final locations of three cardiolipin molecules in the *cyt* bc_1 structure, as observed in our simulations (conf$_4$, cardiolipins yellow with red oxygens). Other lipids are shown only in the background for clarity. In panels b–d are shown close-up snapshots of the CL locations versus the locations observed in the crystal structure by Solmaz et al. ([25], PDB: 3CX5). The yellow CL is the one observed in our MD simulations and the green one is from the crystal structure. The positions were obtained by superimposing the protein structures from MD simulations (colored ribbons) with the crystal structure (gray tubes). Panel c corresponds to simulation conf$_4$, and panels b and d to simulation conf$_1$.

3.2. Cardiolipins diffuse to be an integral part of the protein complex

3.2.1. Cardiolipins bind close to the Q_i-site

When the simulations were started, we readily observed that a CL molecule diffused spontaneously to a particular position in the complex: to the surface of the protein, located on both sides of the protein dimer in the vicinity of the Q_i-site (see Fig. 2 (top)).

The double negatively charged head group of the CL molecule pointed towards the N side (see Fig. 1B), while its hydrophobic acyl tails aligned towards the P side. Importantly, a similar binding location for CL has also been reported in the yeast *cyt* bc_1 crystal structures (PDB: 1KB9; [22]; PDB: 3CX5; [25]), see Fig. 2 (panels B and D). While the yeast and bacterial complexes differ markedly in their amino acid sequence and subunit composition, the CL molecule acquired quite the same positioning near the Q_i-site in both the yeast X-ray structure and in our simulations with the bacterial complex. This is demonstrated in Fig. 2 (panels B and D), which provides compelling evidence for the agreement between simulations and experiments: it is clear that in the simulation model the CLs diffuse spontaneously to the same spots as observed in the crystal structure. All four simulations yielded essentially the same conclusion. The minor difference between the simulations and experiments (Fig. 2) is expected due to, e.g., crystallization conditions and the differences between the yeast and bacterial complexes.

The conserved positioning of CL can largely be explained by electrostatic effects, i.e., the lipid's anionic head group is attracted by the positively charged residues such as lysines and arginines on the protein surface. Nonetheless, since the head group of CL is very small and charged, the conserved positioning can also in part be driven by the so-called umbrella effect, where the head groups of other lipids and the residues of the protein shield the CL hydrophobic part from contact with water. This possibility would deserve further attention in future studies.

Although the CL positioning was very similar on both sides of the dimer, there were differences between the monomers. On the A side, the CL molecule stayed close to the *cyt b* subunit and H-bonded only with TRP44 (Table S1). Closer association of the CL molecule with the *cyt* c_1 subunit on the B side was induced by a number of stable H-bonding interactions: the CL's phosphate groups formed H-bonds with the side chains of ASN246, TYR243 and LYS254 of the *cyt* c_1 subunit (Table S1). It is also noteworthy that in the yeast structures the CL head group resides in a clearly visible niche on the protein surface — an equally tight fit could not happen with the bacterial complex that consists of a minimal *cyt* bc_1 core.

In addition, we found that one CL molecule always occupied a central position close to the Q_i-site(s) between the heme b_H groups of the *cyt b* subunits, the head group pointing towards the N side leaflet. The distance diffused by CL varied between the four simulated system configurations but was typically ~20–25 Å after which its movement became more confined as demonstrated by the small variations in the distance plots (Fig. S2). Altogether, this diffusion process took typically about 20–40 ns.

A similar binding location for CL has also been reported in the yeast *cyt* bc_1 crystal structure (PDB: 3CX5; [25]), see Fig. 2 (panel

C). Although the CL entered the dimer interface in all four simulations (Fig. S2), in two simulations the lipid molecule approached the heme b_H groups in particular ($conf_2$ and $conf_4$, see Fig. S2). Interestingly, despite several similarities, the binding residues differ in the four simulations (Fig. 3). In the $conf_1$ (Fig. 3A, B) and $conf_3$ simulations (Fig. 3D), the CL molecule binds first to LYS12 of the *cyt b* subunit at the side of the cavity. For the $conf_1$ in particular (Fig. 3A, B), the occupancy of this H-bond was 75% over the entire simulation. In the $conf_2$ and $conf_4$ simulations (Fig. 3C and E, respectively), where CL reached deeper inside the dimer interface than in the other two simulations, CL first bonded to ARG22 at the A side and then also to TRP214 at the B side. This linked the two dimer sides together for 69–200 ns of the $conf_2$ simulation and for 113–129 ns of the $conf_4$ trajectory. Later on, the interactions to the A side residues were broken and simultaneously a local conformational shift occurred, widening the dimer interface near the Q_i-site. Fig. 3B–E show parts of the *cyt b* secondary structures from the A (light blue) and B (light red) sides of the dimer (Fig. 1A), represented as transparent cartoon models.

Next we measured the distance of the above-mentioned CL molecules to the b_H hemes to quantitatively estimate their positioning with respect to the Q_i-site (Fig. S3). At the end of the simulations, the distance from the surface-bound CLs to the heme b_H ranged around 22–26 Å for the CL on the B-side of the dimer and around 19–21 Å (somewhat larger in two simulations) for the CL on the A-side. Notably, because the distance was measured between the centers of mass of the CL head group (phosphorus atoms) and the heme b_H, the effective distance could be occasionally even smaller. These distances are equivalent to the values of 19.4–19.5 Å measured from the yeast *cyt* bc_1 complex X-ray crystal structures (PDB: 1KB9 [22], PDB: 3CX5 [25]). For the centrally-located CL, the final CL–heme b_H (B side) distances fluctuated around ~22–24 Å in the $conf_1$ and $conf_2$ simulations. The shortest final distance (~18 Å) was observed in the $conf_4$ simulation. The distance of CL head group to the A side heme b_H was somewhat larger in all simulations. However, the arrangement was almost symmetric between the monomers in the $conf_2$ simulation. The final distances (Fig. S2) are well in line with the crystallographic results calculated from the yeast *cyt* bc_1 structure (PDB: 3CX5; [25]), which have been determined to be 19.7–20.0 Å from the central CL to each of the hemes.

Despite strenuous efforts we did not find any major secondary structure changes such as helix unwinding around the protein complex that would have correlated with CL–protein interactions. Only minor changes in the dimer arrangement at the inner leaflet were observed as a result of CL binding, likely related to the CL entry to the dimer interface.

3.2.2. Conserved cardiolipin binding on the protein surface

To determine the possible conserved CL binding sites on the protein surface, we searched for long-lived CL–protein H-bonds. A limiting value for the occupancy of a long-lived H-bond was calculated based on two criteria: 1) the area per lipid and 2) CL diffusion speed. A preceding computational study [28] suggested that it takes roughly 60 ns (corresponding to H-bond occupancy of 30%) for a CL molecule to move across its own area in the membrane plane. This value was used as a rough estimate for the time it would take for a CL to move a distance of its own size in the bilayer plane. While the time would be longer if the diffusion were considered in the immediate vicinity of the protein [3], we expect this value to adequately describe the average lipid diffusion process.

In line with experimental results [45], the majority of the tightly bound CLs were bound on the N side of the protein and only one CL bound strongly on the positive P side. All CL–protein H-bonds with occupancies over 30% are listed in Table S1, including the CLs near the active sites (discussed above). Of the listed binding locations, the one acquired by CL on the surface of the *cyt* c_1 on the A side (bound in all simulations, binding residues LYS247, ARG248, HIS256 and LYS257) was particularly long-lived, lasting for a major part of all of the 200 ns simulations. This location of CL also induced minor conformational changes (helix reorientation) in two of the simulations. In one simulation, the CL in question formed an H-bond also with the ISP subunit on the B side. Meanwhile, on the A side, there was also a CL molecule close to the equivalent place near the ISP subunit in the starting configuration. It formed an H-bond with the *cyt b* subunit (with residues LYS362 and TRP366) that lasted for a major period of three simulations.

3.2.3. No specific binding pattern for cardiolipin

A specific CL–protein binding pattern, designated as XXY, where one molecule would bind to two positively charged residues (XX) and one polar residue Y, was suggested by Palsdottir and Hunte [45]. Accordingly, there is one bound CL molecule in every simulation that follows this pattern, where CL binds to two positive lysine residues (LYS247 and LYS254 of *cyt* c_1 or LYS251 of *cyt b*) and a polar asparagine residue (ASN42 of *cyt b*) for part of the simulation. The occupancies varied a

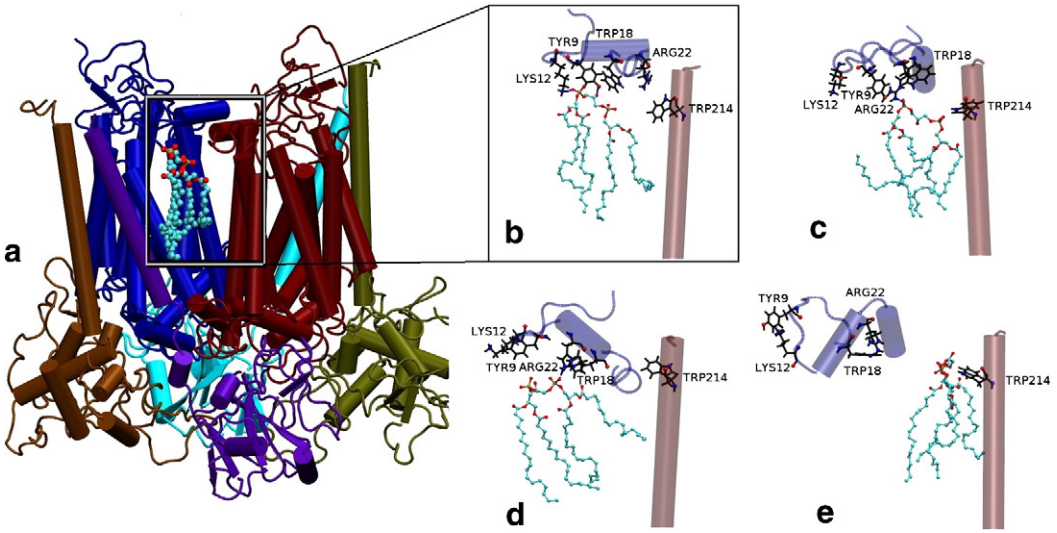

Fig. 3. Cardiolipin binding in the cytochrome bc_1 dimer interface at 200 ns. a) The final positioning of a CL molecule (CPK model with cyan carbons) that entered the dimer interface (cartoon model) from the lipid bilayer (see Fig. 2) during the $conf_1$ simulation (Table 1). b–e) Close-ups of CLs (ball-and stick models with cyan backbone) and their main interacting partners (ball-and-stick models with black backbone) at the dimer interface in the $conf_1$–$conf_4$ simulations. In panels B–E are shown parts of the *cyt b* secondary structures from A (light blue) and B (light red) sides of the dimer (Fig. 1A), shown as transparent cartoon models.

lot between simulations, ranging from 6 to 75% for individual H-bonds. Simultaneous binding to two lysines and one asparagine was observed to happen only momentarily in the $conf_1$, $conf_2$, and $conf_4$ simulations. This binding pattern did not occur with the other CL molecules in any of the simulations, which implies that this suggested arrangement is not generally favored with the membrane-embedded *cyt* bc_1 complex. Altogether, it is fair to say that we did not find a universal binding pattern for CL.

To further examine the CL–protein contacts, we analyzed the H-bonding between CLs and protein residues (Table S2). Via their hydroxyl groups, CLs were observed to H-bond with the protein both as donors and acceptors. Only the H-bonds with occupancies over 1% were considered (as determined in terms of percentage of trajectory frames when the bond exists). The negatively charged CL molecules H-bonded preferentially with positively charged lysine residues (~26% in $conf_1$, $conf_2$, and $conf_4$, see Table S2). This strong preference was evident in all of the simulations except in $conf_3$ where tryptophan residues had a slightly stronger preference (26% in $conf_3$, Table S2). The second favored binding partners were the tryptophan residues forming 18% of all H-bonds on average.

3.3. Cardiolipin positioning close to the Q_i-site suggests a role in proton uptake

The anionic head groups of CL molecules have been proposed to act as proton traps or buffers, supplying protons for the *cyt* bc_1 complex [23]. The idea is that CL would pass a new proton to a nearby lysine side chain from which it would detach during the reduction of ubiquinone [24]. The CL molecules positioned near the Q_i-sites in various *cyt* bc_1 X-ray crystal structures [9–14,22,25,46] indeed support the idea that they could serve as the entry point for the proton uptake process [22,24]. As there is no direct opening between the enzyme's Q_i-site and the bulk solvent, this short proton 'wire' or a hydrogen-bonded network is needed [22,24]. Such a network, called the CL/K pathway, was described in [24] to consist of CL bound to the *cyt b* surface, a lysine residue (LYS228 in yeast *cyt* bc_1 crystal structure; PDB: 1KB9), and three water molecules (Fig. 4A).

Notably, the CL arrangement at the site in the yeast bc_1 crystal structure (Fig. 4A, [24]) is very similar to the one seen for the bacterial complex at the end stage of our simulations (Fig. 4A, B). In line with this proton uptake hypothesis, the positioning of water molecules and the LYS251 side chain in our simulations indeed suggest a possible proton uptake pathway between the CL molecule and the bound quinone/semiquinone at the Q_i-site (Fig. 4B). Even though all the H-bonds comprising this network did not generally exist precisely at the same time, the similar chain-like arrangement existed in the different simulations. Qualitatively, the described arrangement is seen during 80–200 ns ($conf_1$) and 110–200 ns ($conf_1$ and $conf_2$, where for part of the time CL is bound straight to LYS251). In the $conf_3$ simulation the CLs are located slightly further away from the lysine, accommodating at least two water molecules between the head group and the lysine side chain. We wish to note that even though the discussion above only concerns the surface-bound CLs, it is possible that the centrally-located CL, also positioned close to the active sites, may also form a proton-uptake pathway with water molecules between its binding site and the active site.

The proximity of the CL head group affected the local electrostatic potential near the proposed entrance to the proton conduction pathway (Fig. 5). The electrostatic potential differs between the beginning of the simulation, when the lipid molecules have not yet bound to the protein surface, and the end stage when the system is equilibrated. There was a general shift towards neutral/negative potential values on the N side during the simulation, but also a specific effect by the bound CL molecules at the Q_i-site (circled areas in Fig. 5). However, this is not always the case since other factors such as the orientation of protein residues and the binding of counter ions also contribute. Fig. 4C gives a qualitative look at the potential of the proposed proton conduction pathway, where the potential of the whole system is reflected on the molecular surfaces of the suggested proton transfer partners. Notably, the CL head group, which has been suggested to act as a proton trap, concentrating protons to the bilayer surface and passing them further to the protein [24], reflects a clearly negative potential.

3.4. Behavior of other phospholipids

Like CLs with their hydroxyl groups, PEs are also able to participate in H-bonding as proton donors via their ammonium groups, whereas PCs can act only as acceptors (Fig. S1). In the simulations PCs and PEs formed a greater number of shorter-lived H-bonds than the more negatively charged CLs. During the last 10 ns of the simulations, CLs formed on average seven H-bonds with protein residues at each time step, as PCs form 23 and PEs 24. Thus, CL–protein H-bonding accounts for 13% of all H-bonds at a given time step, while PCs account for 42%, and PEs for 45% of the H-bonds. The corresponding molar concentrations for CL, PC, and PE in the membrane are 12, 48, and 40%, respectively. The H-bonds of PCs and PEs had shorter lifetimes compared to those formed by CL, the average occupancies being 20, 9, and 14% for CL, PC, and PE, respectively. A slight preference for lysine residues is seen also for PC and PE. However, it is not as clear as in the case of CL, see Table S3. Other favored H-bonding partners were tryptophan, asparagine, and tyrosine for PCs, and arginine, serine, and aspartic acid for PEs. The conserved binding sites of PC and PE were analyzed similarly as those of CL (Table S3). Due to the great number of these bonds, the selection was further refined to include only H-bonds that were found in at least three out of the four simulations. Interestingly, half of the H-bonds

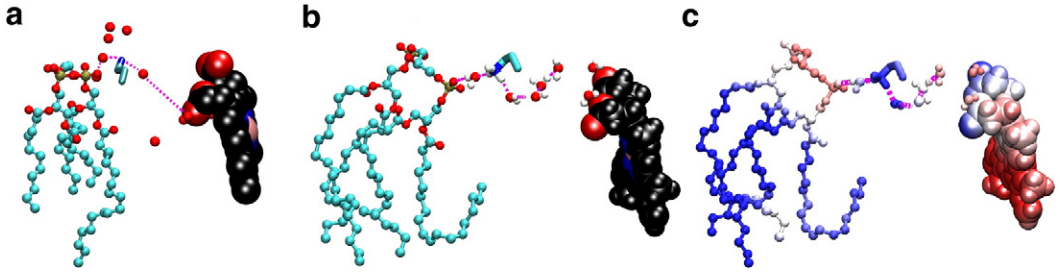

Fig. 4. Possible water-mediated proton-uptake pathway involving cardiolipin near the Q_i-site. a) A water bridge between a CL molecule (ball-and-stick model with cyan carbons, red oxygens and brown phosphates) and heme b_H (CPK model with black backbone) close to the Q_i-site (see Fig. 1A) in the yeast *cyt* bc_1 complex crystal structure (PDB: 1KB9; [22]. The protein is omitted for clarity and only the side chain of the lysine (LYS228) taking part in the conduction pathway is shown (stick-model, carbons cyan, nitrogen blue). The proposed hydrogen-bonded proton transfer pathway from cardiolipin to the water molecule in the Q_i-site is shown with magenta dotted lines. b) Similar arrangement of water was reproduced for example in the end of the $conf_1$ simulation (snapshot taken at 199.25 ns). Water hydrogens (white) are only shown in the MD simulation snapshot (panel b). H-bonds existing at this time step are shown with dotted magenta lines. The side chain of LYS251 is shown as a stick model (hydrogens white). c) The same arrangement as in panel B but colored according to the electrostatic potential of the system. The potential values were calculated based on all atoms in the system and averaged over the last 1 ns of the simulation. Red color indicates negative potential values, blue indicates positive, and white corresponds to neutral.

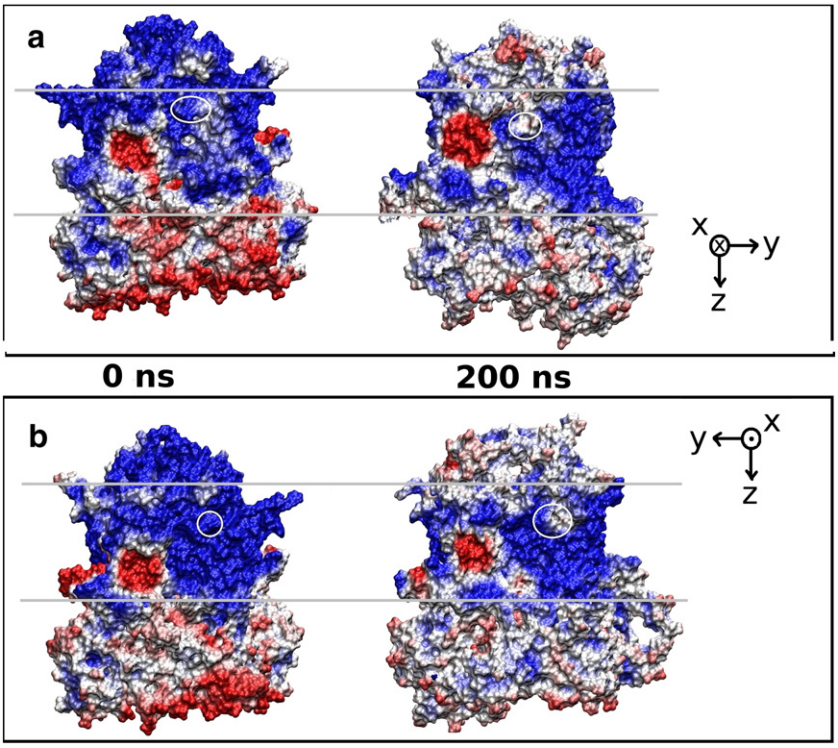

Fig. 5. Electrostatic potential on protein surface. Comparison of snapshots from the beginning and end of the simulation, two sides (on panels a and b) of the protein shown. The phospholipid membrane (level of head group phosphates) is indicated by the gray lines. The N side of the membrane points up, as indicated by the axes on the right. The protein is shown as a van der Waals-surface (probe radius 1.4 Å). The white circles mark the sites of given cardiolipin molecules on the A side of $conf_1$ (a) and on the B side of $conf_2$ (b) of the dimer (see Fig. 1B). The values of the electrostatic potential on the protein surface are shown with the blue color indicating positive values and red color indicating negative. White color indicates the zero potential. The shown potentials are averages over 1 ns time slices, e.g. the first snapshot shows the average potential during 0–1 ns of the simulation and the second shows the average potential during 199–200 ns. All atoms in the system were taken into account when calculating the potential.

found were those of lipids from the P side rather than from the N side, as was the case with the tightly bound CLs.

PEs and PCs, in addition to CL (Fig. 3), also entered the dimer interface during the simulations. In the starting configuration, a PC molecule (head group pointing to the N side) lied straight between CL and the protein and consequently the two lipids moved together to the cavity. As opposed to the CL molecule, PC formed hardly any H-bonds on its way inside. The head group of PC ended up closer to the monomer B than to the monomer A in all simulations (Fig. S4, Fig. 1A). Steric interactions are expected to play a role in this arrangement of the lipids rather than the electrostatic ones. On the other side, there were PE molecules (head groups pointing to the N side), which were initially located closer to the protein than either CL or PC. These PEs (shown for the B side in Fig. S5) H-bonded with the residues lining the cavity near the protein surface, while their acyl chains penetrated deep into the protein (Fig. S5B). This is evidenced by a smaller PE tails–heme b_H distance as compared to the PE head–heme b_H distance (Fig. S5A), resulting in some cases in an almost horizontal orientation of the lipid (Fig. S5B).

The lipids entering the dimer interface from the two opposite sides of the membrane and enclosing the *cyt* bc_1 complex moved deep into the protein complex and ended up being very close to each other. The distance between the central glycerol atoms of CL and PE changed from 70 Å in the initial configuration to ~20 Å in the end of the simulations, and the tails of lipids from the opposite sides were touching in the $conf_2$ and $conf_4$ set-ups. The head groups of all phospholipids were positioned on the N side. Since these lipids interacted with both monomers of *cyt* bc_1, they should substantially affect the stability of the dimer interface and could also be involved in dimer formation. An interesting feature of this lipid network is the acyl chain disorder which has been previously suggested to provide a pathway for quinone/quinol diffusion and exchange between the lipid bilayer and the inter-monomer cavity in the bc_1 complex [47].

3.5. The dimer complex opens on the P side of the membrane

The *cyt* bc_1 complex was observed to undergo rearrangement at the dimer interface on the P side in all of the 200 ns simulations. The P side parts of the *cyt* c_1 subunits moved the most (Fig. S8D). This view was supported by both a visual inspection of the simulation trajectories (Fig. 1C vs. D) and calculation of the prosthetic redox center distances (Fig. S6A–D, Table S4). The distances between the equivalent heme c_1 groups across the dimer interface also increased (Fig. S6D, Table S4). The conformational shift took place due to non-specific electrostatic lipid–protein interactions that were not present in the initial crystal structure, i.e., the positively charged residues aligned favorably towards the hydrophilic head groups of the lipid membrane (Fig. 1B). Despite these changes, the core of the enzyme remained fairly immobile as shown by the moderate ~1–2 Å increase in the heme b_L distance across the dimer interface (Fig. S6A, Table S4). Furthermore, the calculations on the solvent accessible surface area (SASA) showed that the contact area between the *cyt b* subunits increased markedly in most of the simulations.

Moreover, the opening of the dimer interface on the P side was more pronounced in the Q_o-site simulations lacking a bound substrate ($conf_1$, $conf_{12}$, Table S4) than what was seen in the substrate-occupied simulations ($conf_3$, $conf_4$, Table S4). This widening was accompanied by narrowing of the dimer interface close to the Q_i-site or the N side in the *apo*-Q_o simulations (Fig. 1B). This was shown by the heme b_H distance across the dimer interface (Table S4). Accordingly, the results suggest that the substrate binding at the Q_o-site could weaken the extent of the movements of the extracellular domain, as the spreading on the P side was most prominent in the *apo*-Q_o simulations (Fig. 1B). A plausible mechanism behind the increased widening in the *apo* simulations could be the lack of a bound substrate to mediate specific *cyt b*-ISP subunit interactions, as was the case in the substrate-occupied simulations [32].

A close association of *cyt b* and ISP subunits is needed for the successful reaction cycle at the Q_o-site [9]. However, the transfer of electrons from the Fe_2S_2 cluster to the heme c_1 is equally important. To facilitate the transfer, the ISP and *cyt* c_1 subunits have to stay close to each other. In our case, on average, the Fe_2S_2 cluster-heme c_1 distances did not change within the dimer sides or across the dimer interface (Table S5). However, a closer inspection showed that the redox center distance fluctuated above and below the initial crystal structure value on the A and B sides, respectively (Fig. S7, Table S5). Similarly, the contact surface area between ISP and *cyt* c_1 subunits on either dimer side was raised only slightly and differed widely between simulations and dimer sides (Table S5). Because these domain movements did not seem to follow a similar pattern on the dimer sides in any of the simulations, it seems unlikely that substrate-occupancy at the Q_o-site could be the governing factor behind the extracellular ISP-*cyt* c_1 association.

4. Discussion

From structural point of view, the simulation results stress the membrane protein nature of the *cyt* bc_1 complex and consequently one should remain wary when examining it out of this context. Although several experimental studies have successfully demonstrated that specific lipids are an integral part of the dimer complex [10,25,45], the X-ray crystal structures have been unable to depict the full effect of the surrounding lipid bilayer on the enzyme's quaternary structure. The existing structures are likely accurate in describing the enzyme's protein fold at the monomer level [31], but due to the lack of large-scale lipid–protein contacts the solved dimer assemblies appear to be somewhat distorted. When the bc_1 dimer was simulated in a lipid bilayer, the dimer interface opened considerably on the P side leaflet immediately in all of our simulations (Fig. 1C vs. D). The driving force behind the conformational shift was the electrostatic effect of the bilayer: the positively charged residues of the P side domains spread out to acquire more favorable alignment against the negatively charged phosphate groups of the phospholipids.

Prior to this work, we have already demonstrated through atomistic simulations that quinol binding accompanied by coordinated water arrangement at the Q_o-site assures exceptionally close association of the extracellular domains of the *cyt b* and ISP subunits [32]. This arrangement is a prerequisite for the electron transfer to the Fe_2S_2 cluster during the oxidation of quinol [9]. However, the electron transfer should also continue towards the heme c_1 on the high-potential chain (quinol → Fe_2S_2 cluster → heme c_1). None of our simulations recreated the full range of ISP movement in relation to the *cyt b* subunit seen in the crystal structures. Yet also the Fe_2S_2 cluster-heme c_1 distance fluctuated above and below the initial crystal structure value (Fig. S6, Table S7). This suggests that the distance between *cyt* c_1 subunits and ISP subunits might change randomly back and forth independent of the Q_o-site interactions. On the other hand, the final dimer assembly at the P side (Fig. 1C, D) differed considerably between the substrate-occupied and ligand-free Q_o simulations. Without a bound ligand at the Q_o-site, the dimer interface widened more at the P side than in the Q_o-occupied simulations. In other words, the monomer parts approached each other a little bit near the N side leaflet. Thus, it seems that the substrate binding at the Q_o-site not only influences the *cyt b*-ISP dynamics but it also affects inter-monomer dynamics.

The dimer interface on the N side leaflet, covering the vicinity of the Q_i-site, became filled by a variety of phospholipids during the first 50 ns of our simulations. Previous X-ray crystallization studies have already suggested that the cavity contains phospholipids [25,45]. However, the atomistic simulations show conclusively that the entire space is filled with lipids. Although more lipids entered the dimer interface in the simulations than is seen in the available structures, it is possible that the cavity could contain a few more phospholipids in situ. Because of the delayed entry of phospholipids, solvent molecules also entered the area of the cavity, where presumably only lipids should reside. This solvation prevented unwanted vacuum effects inside the dimer interface in the very beginning of the simulations. On the other hand, the inflowing lipids were mostly able to displace the water molecules in the cavity. Even though the entered lipids must have a structural role keeping the dimer sides of the *cyt* bc_1 complex apart (Fig. 1A), no hefty movements (only local changes) between the dimer sides (e.g., redox center distance changes) could be attributed directly to specific lipid effects.

We detected two specific CL binding sites for the *cyt* bc_1 complex of *R. capsulatus* in our MD simulations: 1) in the dimer interface and 2) on the surface of the protein outside the interface. Both positions are close enough to the Q_i-site to possibly affect its function. Notably, the CL binding site(s) outside the dimer interface has (have) been suggested to function in the proton uptake [22,24]. In general, the entry of the lipid molecules into the dimer interface seemed to be directed by hydrophobic or steric interactions, but with CL the negatively charged head group also affected its final positioning. Initially the electrostatic potential of the dimer interface was neutral, favoring the entry of hydrophobic acyl tails of phospholipids. However, the later changes in the cavity implied that the potential became more positive, thus attracting especially the doubly negative CL head group. Although there were minor differences in the composition and positioning of the lipids that entered the dimer interface during the simulations, CLs consistently acquired these conserved positions close to the Q_i-site.

The consistency in the CL positioning both in our simulations and in previous structural studies supports the hypothesis of CLs participating in the proton uptake from the N side to the redox reactions at the Q_i-sites [45]. The positioning of CL at the dimer interface was first reported by Palsdottir and Hunte [45] based on electron density data, followed by another study showing CL at the same site [25]. Thus, our simulations support previous experimental results indicating the CL's central positioning in the *cyt* bc_1 dimer interface. The simulations were also able to reproduce the X-ray crystallization results regarding CL positioning outside the dimer interface. That is to say, a CL molecule bound close to the heme b_H on both monomers in almost all of our simulations, in line with several crystallization studies for different species. Our simulation results therefore provide quite compelling evidence that these CL binding sites are conserved regardless of the origin of the *cyt* bc_1 complex inspected. Positioning of a CL molecule in a central location and in the vicinity of the heme b_H has also been observed in a coarse grained MD study of bovine and yeast *cyt* bc_1 complexes [48]. The next logical question is whether the preference for CLs at these sites has direct effects on the Q-cycle, or if CLs only affect the *cyt* bc_1 complex integrity or dimer arrangement.

The negatively charged head groups of CLs, positioned on the sides of the monomers, are connected by a lysine residue and a water meshwork to the Q_i-site (Fig. 4). This arrangement could render water-mediated proton tunneling possible between the CL molecules and the non-protonated substrates. Interestingly, also another respiratory complex has been predicted to have a CL binding site at the entrance of a proton uptake pathway [49]. Unfortunately, the simulations cannot conclusively confirm the role of either central or peripheral CL molecules in the proton transfer. We analyzed exhaustively the effect of CLs on the electrostatic potential of the *cyt* bc_1 complex, and especially concentrated on the vicinity of the Q_i-site. It is clear that the CL molecules that acquired these conserved positions can in some cases shift the electrostatic potential to more negative values, in principle therefore attracting protons from the N side (Fig. 5). It is possible that the real differences in the electrostatic potential did not show in our simulations because the dimer interface lacked some lipids, and, thus, the Q_i-site was not isolated enough from the water phase. However, the fact that both MD simulations and crystallographic studies positioned CL molecules in these particular sites (at the periphery and at the dimer interface of the *cyt* bc_1 complex) provides a strong indication that these CL–protein interactions close to the Q_i-site are universally conserved.

5. Conclusions

The atomistic molecular dynamics simulations reported here provide a great deal of insight into understanding the role of cardiolipin (CL) in *cyt* bc_1 complexes. It provides one with an alternative refined dimer arrangement for the *cyt* bc_1 dimer at the P side leaflet of the membrane (see Fig. 1B). The picture suggested here differs somewhat from the previous X-ray crystallographic data. The new tertiary assembly of the protein dimer is caused by non-specific lipid–protein interactions such as hydrophobic and electrostatic effects. The simulations also provide clear-cut evidence that phospholipids and in particular CLs are an integral part of the *cyt* bc_1 complex at the dimer interface. In contrast to previous X-ray crystallization studies which have suggested the cavity to contain only a few phospholipids, the atomistic simulations show conclusively that the entire space is filled with lipids. Interestingly, the entered lipid position themselves in the close vicinity of the heme b_H groups in the Q_i-site. Although the composition and alignment of the entered lipids varied slightly between the simulations, each time there was a CL molecule, which spontaneously diffused to a central location inside the cavity. Importantly, the observed central positioning of CL inside the dimer is consistent with the previous X-ray crystallographic data [25,45]. Also, outside the dimer interface CLs were able to acquire close positions to the heme b_H groups on the protein surface as reported in several crystal structures. The consistency in the CL positioning in the close vicinity of the Q_i-site in our simulations and in previous X-ray crystallographic studies suggests that the negatively charged phospholipid species could indeed function as a proton source during substrate quinone/semiquinone reduction [22,23]. Overall, the conserved CL positioning near the Q_i-site suggests that the lipid has a central role in the *cyt* bc_1 complex structure and possibly in the redox reactions too.

Acknowledgments

Computational resources were provided by the Finnish IT Centre for Science (CSC). We acknowledge that the results of this research have been in part achieved using the PRACE-2IP project (FP7 RI-283493) resource Lindgren based in Sweden at PDC. For financial support, we wish to thank the Academy of Finland (TR, IV, PAP), Finnish Doctoral Programme in Computational Sciences (SP, KK) and Vilho, Yrjö and Kalle Väisälä Foundation (SP) for financial support, and the European Research Council through the Advanced Grant (CROWDED-PRO-LIPIDS). AO acknowledges The Welcome Trust International Senior Research Fellowship.

Appendix A. Supplementary data

Supplementary data to this article can be found online at http://dx.doi.org/10.1016/j.bbabio.2013.03.005.

References

[1] D. Lingwood, K. Simons, Lipid rafts as a membrane-organizing principle, Science 327 (2010) 46–50.
[2] A.G. Lee, How lipids affect the activities of integral membrane proteins, Biochim. Biophys. Acta 1666 (2004) 62–87.
[3] P.S. Niemelä, M.S. Miettinen, L. Monticelli, H. Hammaren, P. Bjelkmar, T. Murtola, E. Lindahl, I. Vattulainen, Membrane proteins diffuse as dynamic complexes with lipids, J. Am. Chem. Soc. 132 (2010) 7574–7575.
[4] R. Phillips, T. Ursell, P. Wiggins, P. Sens, Emerging roles for lipids in shaping membrane–protein function, Nature 459 (2009) 379–385.
[5] F.-X. Contreras, A.M. Ernst, P. Haberkant, P. Björkholm, E. Lindahl, B. Gönen, C. Tischer, A. Elofsson, G. von Heijne, C. Thiele, R. Pepperkok, F. Wieland, B. Brügger, Molecular recognition of a single sphingolipid species by a protein's transmembrane domain, Nature 481 (2012) 525–529.
[6] C. Hunte, S. Richers, Lipids and membrane protein structures, Curr. Opin. Struct. Biol. 18 (2008) 406–411.
[7] H. Schägger, T. Hagen, B. Roth, U. Brandt, T.A. Link, G. von Jagow, Phospholipid specificity of bovine heart bc1 complex, Eur. J. Biochem. 190 (1990) 123–130.
[8] C.A. Yu, L. Yu, Structural role of phospholipids in ubiquinol–cytochrome c reductase, Biochemistry 19 (1980) 5715–5720.
[9] Z. Zhang, L. Huang, V.M. Shulmeister, Y.I. Chi, K.K. Kim, L.W. Hung, A.R. Crofts, E.A. Berry, S.H. Kim, Electron transfer by domain movement in cytochrome bc1, Nature 392 (1998) 677–684.
[10] H. Palsdottir, C.G. Lojero, B.L. Trumpower, C. Hunte, Structure of the yeast cytochrome bc1 complex with a hydroxyquinone anion Qo site inhibitor bound, J. Biol. Chem. 278 (2003) 31303–31311.
[11] L.-S. Huang, D. Cobessi, E.Y. Tung, E.A. Berry, Binding of the respiratory chain inhibitor antimycin to the mitochondrial bc1 complex: a new crystal structure reveals an altered intramolecular hydrogen-bonding pattern, J. Mol. Biol. 351 (2005) 573–597.
[12] E.A. Berry, L.-S. Huang, D.-W. Lee, F. Daldal, K. Nagai, N. Minagawa, Ascochlorin is a novel, specific inhibitor of the mitochondrial cytochrome bc1 complex, Biochim. Biophys. Acta 1797 (2010) 360–370.
[13] E.A. Berry, Z. Zhang, H.D. Bellamy, L. Huang, Crystallographic location of two Zn(2+)-binding sites in the avian cytochrome bc(1) complex, Biochim. Biophys. Acta 1459 (2000) 440–448.
[14] L. Esser, B. Quinn, Y.-F. Li, M. Zhang, M. Elberry, L. Yu, C.-A. Yu, Di Xia, Crystallographic studies of quinol oxidation site inhibitors: a modified classification of inhibitors for the cytochrome bc(1) complex, J. Mol. Biol. 341 (2004) 281–302.
[15] T. Wenz, R. Covian, P. Hellwig, F. Macmillan, B. Meunier, B.L. Trumpower, C. Hunte, Mutational analysis of cytochrome b at the ubiquinol oxidation site of yeast complex III, J. Biol. Chem. 282 (2007) 3977–3988.
[16] T. Wenz, R. Hielscher, P. Hellwig, H. Schägger, S. Richers, C. Hunte, Role of phospholipids in respiratory cytochrome bc(1) complex catalysis and supercomplex formation, Biochim. Biophys. Acta 1787 (2009) 609–616.
[17] M. Fry, D.E. Green, Cardiolipin requirement for electron transfer in complex I and III of the mitochondrial respiratory chain, J. Biol. Chem. 256 (1981) 1874–1880.
[18] B. Gomez, N.C. Robinson, Phospholipase digestion of bound cardiolipin reversibly inactivates bovine cytochrome bc1, Biochemistry 38 (1999) 9031–9038.
[19] F. Hoch, Cardiolipins and biomembrane function, Biochim. Biophys. Acta 1113 (1992) 71–133.
[20] M. Schlame, D. Rua, M.L. Greenberg, The biosynthesis and functional role of cardiolipin, Prog. Lipid Res. 39 (2000) 257–288.
[21] M. Zhang, E. Mileykovskaya, W. Dowhan, Gluing the respiratory chain together. Cardiolipin is required for supercomplex formation in the inner mitochondrial membrane, J. Biol. Chem. 277 (2002) 43553–43556.
[22] C. Lange, J.H. Nett, B.L. Trumpower, C. Hunte, Specific roles of protein–phospholipid interactions in the yeast cytochrome bc1 complex structure, EMBO J. 20 (2001) 6591–6600.
[23] T.H. Haines, N.A. Dencher, Cardiolipin: a proton trap for oxidative phosphorylation, FEBS Lett. 528 (2002) 35–39.
[24] C. Hunte, H. Palsdottir, B.L. Trumpower, Protonmotive pathways and mechanisms in the cytochrome bc1 complex, FEBS Lett. 545 (2003) 39–46.
[25] S.R.N. Solmaz, C. Hunte, Structure of complex III with bound cytochrome c in reduced state and definition of a minimal core interface for electron transfer, J. Biol. Chem. 283 (2008) 17542–17549.
[26] S. Nichols-Smith, T. Kuhl, Electrostatic interactions between model mitochondrial membranes, Colloids Surf. B Biointerfaces 41 (2005) 121–127.
[27] M. Dahlberg, A. Marini, B. Mennucci, A. Maliniak, Quantum chemical modeling of the cardiolipin headgroup, J. Phys. Chem. A 114 (2010) 4375–4387.
[28] S. Pöyry, T. Róg, M. Karttunen, I. Vattulainen, Mitochondrial membranes with mono- and divalent salt: changes induced by salt ions on structure and dynamics, J. Phys. Chem. B 113 (2009) 15513–15521.
[29] M. Dahlberg, A. Maliniak, Molecular dynamics simulations of cardiolipin bilayers, J. Phys. Chem. B 112 (2008) 11655–11663.
[30] D. Aguayo, F.D. González-Nilo, C. Chipot, Insight into the properties of cardiolipin containing bilayers from molecular dynamics simulations, using a hybrid all-atom/united-atom force field, J. Chem. Theory Comput. 8 (2012) 1765–1773.
[31] K. Kaszuba, P.A. Postila, O. Cramariuc, M. Sarewicz, A. Osyczka, I. Vattulainen, T. Róg, Parameterization of the prosthetic redox centers of the bacterial cytochrome bc1 complex for atomistic molecular dynamics simulations. Theoretical Chemistry Accounts. in press.
[32] P.A. Postila, K. Kaszuba, M. Sarewicz, A. Osyczka, I. Vattulainen, T. Róg, Key role of water in proton transfer at the Qo-site of the cytochrome bc1 complex predicted by atomistic molecular dynamics simulations. BBA Bioenerg. in press, http://dx.doi.org/10.1016/j.bbabio.2013.02.005.
[33] E.A. Berry, L.-S. Huang, L.K. Saechao, N.G. Pon, M. Valkova-Valchanova, F. Daldal, X-ray structure of *Rhodobacter capsulatus* cytochrome bc (1): comparison with its mitochondrial and chloroplast counterparts, Photosynth. Res. 81 (2004) 251–275.
[34] W. Humphrey, A. Dalke, K. Schulten, VMD: visual molecular dynamics, J. Mol. Graph. 14 (1996) 33–38, (27–8).
[35] T. Róg, H. Martinez-Seara, N. Munck, M. Oresic, M. Karttunen, I. Vattulainen, Role of cardiolipins in the inner mitochondrial membrane: insight gained through atom-scale simulations, J. Phys. Chem. B 113 (2009) 3413–3422.
[36] J.C. Phillips, R. Braun, W. Wang, J. Gumbart, E. Tajkhorshid, E. Villa, C. Chipot, R.D. Skeel, L. Kalé, K. Schulten, Scalable molecular dynamics with NAMD, J. Comput. Chem. 26 (2005) 1781–1802.
[37] A.D. Mackerell, M. Feig, C.L. Brooks, Extending the treatment of backbone energetics in protein force fields: limitations of gas-phase quantum mechanics in reproducing protein conformational distributions in molecular dynamics simulations, J. Comput. Chem. 25 (2004) 1400–1415.
[38] J. Taylor, N.E. Whiteford, G. Bradley, G.W. Watson, Validation of all-atom phosphatidylcholine lipid force fields in the tensionless NPT ensemble, Biochim. Biophys. Acta 1788 (2009) 638–649.

[39] K. Kaszuba, T. Róg, K. Bryl, I. Vattulainen, M. Karttunen, Molecular dynamics simulations reveal fundamental role of water as factor determining affinity of binding of beta-blocker nebivolol to beta(2)-adrenergic receptor, J. Phys. Chem. B 114 (2010) 8374–8386.
[40] U. Essmann, L. Perera, M.L. Berkowitz, T. Darden, H. Lee, L.G. Pedersen, A smooth particle mesh Ewald method, J. Chem. Phys. 103 (1995) 8577.
[41] J.V. Lehtonen, D.-J. Still, V.-V. Rantanen, J. Ekholm, D. Björklund, Z. Iftikhar, M. Huhtala, S. Repo, A. Jussila, J. Jaakkola, O. Pentikäinen, T. Nyrönen, T. Salminen, M. Gyllenberg, M.S. Johnson, BODIL: a molecular modeling environment for structure–function analysis and drug design, J. Comput. Aided Mol. Des. 18 (2004) 401–419.
[42] A. Aksimentiev, K. Schulten, Imaging alpha-hemolysin with molecular dynamics: ionic conductance, osmotic permeability, and the electrostatic potential map, Biophys. J. 88 (2005) 3745–3761.
[43] P.J. Kraulis, MOLSCRIPT: a program to produce both detailed and schematic plots of protein structures, J. Appl. Crystallogr. 24 (1991) 946–950.
[44] E.A. Merritt, M.E.P. Murphy, Raster3D Version 2.0. A program for photorealistic molecular graphics, Acta Crystallogr. D: Biol. Crystallogr. 50 (1994) 869–873.
[45] H. Palsdottir, C. Hunte, Lipids in membrane protein structures, Biochim. Biophys. Acta 1666 (2004) 2–18.
[46] P.J. Crowley, E.A. Berry, T. Cromartie, F. Daldal, C.R.A. Godfrey, D.-W. Lee, J.E. Phillips, A. Taylor, R. Viner, The role of molecular modeling in the design of analogues of the fungicidal natural products crocacins A and D, Bioorg. Med. Chem. 16 (2008) 10345–10355.
[47] C. Hunte, Specific protein–lipid interactions in membrane proteins, Biochem. Soc. Trans. 33 (2005) 938–942.
[48] C. Arnarez, J.-P. Mazat, J. Elezgaray, S.-J. Marrink, X. Periole, Evidence for cardiolipin binding sites on the membrane-exposed surface of the cytochrome bc1, J. Am. Chem. Soc. 135 (8) (2013) 3112–3120, http://dx.doi.org/10.1021/ja310577u.
[49] C. Arnarez, S.-J. Marrink, X. Periole, Identification of cardiolipin binding sites on cytochrome c oxidase at the entrance of proton channels, in press, http://dx.doi.org/10.1038/srep01263.